ZONE BASED GLRT FOR DETECTING PHYSICAL RANDOM ACCESS CHANNEL SIGNALS IN 5G

A THESIS SUBMITTED TO
THE GRADUATE SCHOOL OF ENGINEERING AND SCIENCE
OF BILKENT UNIVERSITY
IN PARTIAL FULFILLMENT OF THE REQUIREMENTS FOR
THE DEGREE OF
MASTER OF SCIENCE
IN
ELECTRICAL AND ELECTRONICS ENGINEERING

By
Feridun Tütüncüoğlu
December 2019

Zone based GLRT for Detecting Physical Random Access Channel Signals in 5G

By Feridun Tütüncüoğlu

December 2019

We certify that we have read this thesis and that in our opinion it is fully adequate, in scope and in quality, as a thesis for the degree of Master of Science.

Orhan Arıkan (Advisor)

Sinan Gezici (Co-Advisor)

Nail Akar

Berkan Dülek

Approved for the Graduate School of Engineering and Science:

Ezhan Karaşan
Director of the Graduate School

ABSTRACT

ZONE BASED GLRT FOR DETECTING PHYSICAL RANDOM ACCESS CHANNEL SIGNALS IN 5G

Feridun Tütüncüoğlu
M.S. in Electrical and Electronics Engineering
Advisor: Orhan Arıkan
Co-Advisor: Sinan Gezici
December 2019

In LTE/5G systems, the random access channel (RACH) process occurs during the boot-up phase. As channel state information is not available at this stage, detecting several devices with high performance presents a challenging problem. In particular, servicing many devices simultaneously can get difficult when a large number of user equipment and machines exist in the network. The problem can become more dramatic as the number of user equipment increases around the world. In the literature, power delay profile (PDP) is proposed as a decision metric for this problem. The use of this metric handles many cases with satisfactory performance and low complexity; however, it does not lead to optimal detection performance. In this thesis, we address this issue with a generalized likelihood ratio test (GLRT) based approach and propose detectors with high detection performance. We also derive an ideal detector that provides an upper bound on the detection probability. Via extensive RACH simulations, it is shown that improvements in detection performance can be achieved by the proposed approach in various scenarios.

Keywords: 5G, detection, GLRT, RACH, Zadoff-Chu sequence.

ÖZET

5G'DE FİZİKSEL RASTGELE ERİŞİM KANAL SİNYALLERİ İÇİN BÖLGE BAZLI GLRT

Feridun Tütüncüoğlu
Elektrik ve Elektronik Mühendisliği, Yüksek Lisans
Tez Danışmanı: Orhan Arıkan
İkinci Tez Danışmanı: Sinan Gezici
Aralık 2019

LTE/5G sistemlerinde rastgele erişim kanalı (RACH) prosesi, kullanıcı ekipmanının ilk açılma fazında gerçekleşir. Bu aşamada kanal durum bilgisi mevcut olmadığından, birden fazla cihazı yüksek performansla tespit etmek zor bir problem haline gelmektedir. Özellikle şebekede fazla sayıda kullanıcı ekipmanı ve makine bulunduğunda, çok sayıda cihaza aynı anda servis sağlamak zorlaşabilmektedir. Bu problem, dünya çapındaki kullanıcı ekipmanı arttıkça daha da çarpıcı hale gelmektedir. Literatürde bu problem için güç gecikme profili (PDP), bir karar metriği olarak önerilmektedir. Bu metriğin kullanılması birçok durumda memnun edici performans ve düşük karmaşıklık sağlamakta fakat optimal sezim performansına ulaştırmamaktadır. Tezde bu hususu, genelleştirilmiş olasılık oranı testi (GLRT) tabanlı bir yaklaşım ile çözmekte ve yüksek sezim performansına sahip seziciler önermekteyiz. Ayrıca sezim olasılığına üst sınır sağlayan bir ideal sezici çıkarmaktayız. Detaylı RACH benzetimleri yoluyla, önerilen yaklaşımla sezim performansında çeşitli senaryolarda elde edilen gelişimler gösterilmektedir.

Anahtar sözcükler: 5G, sezim, GLRT, RACH, Zaddoff-Chu dizisi.

Acknowledgement

First of all, I would like to thank my advisor Prof. Orhan Arıkan and my co-advisor Prof. Sinan Gezici from bottom of my heart. They encouraged, guided and supported me through this research. They kept answering my exhaustive questions with a huge patience, and leaded me to progress through this research. I express my gratitude to them for making this research and thesis possible.

Secondly, I would like to thank my life-long girlfriend Serap Dalmızrak, who has always supported and tolerated me during this research. I also need to thank my father, my mother for their valuable life experiences and their support. I would like to add a speacial thanks to my little brother for his endless support and faith in me.

Lastly, I would like to thank Bilkent University, all my professors, Electrical & Electronics Engineering staff, who contributed to me during this master's degree.

Contents

List of Figures

Chapter 1

Introduction

1.1 Evolution of Mobile Communication

Mobile communication has made a tremendous progress in last a few decades. This type of communication presents many challenges such as undesirable channel conditions, high data rate and low latency requirements and, most importantly requirements for high user capacity per cell to optimize installation cost of internet service providers and user capacity [2], [3]. As can be deduced from the naming strategy, the mobile communication generations started from the first generation (1G) and evolved to 4G or LTE (Long Term Evolution). When standardization institutions standardized 4G, it was known that this would be a long developing process. Therefore, the early stages of 4G are also known as LTE. Every progress made for mobile communication has been included through releases published by 3GPP (Third Generation Partnership Project) [4]. In every release, new standards come or new procedures and methods might be proposed and standardized for mobile communication. In the last several years, 5G has started to be the focus point of research since most of the 4G requirements are met currently. 5G is also called as new radio (NR). The reason behind is that 5G has many different aspects compared to the previous mobile communication generations. The most important and intriguing aspects of NR are given as follows:

- Improved security in the wireless network
- Lower battery consumption and ability to support green mobile communication networks
- Up to 1 Gbps downlink data rate
- Beam-forming and massive MIMO applications
- Enhanced IoT support
- Very low latency requirements to support autonomous cars, and smart factories
- High spectral efficiency
- Improved cell edge coverage

More information and aspects of 5G can be found in the following resources [5], [6], [7], [8], [9].

1.2 Uplink Synchronization in 5G

1.2.1 Problem Definition

This thesis mainly addresses detector performance problems encountered in 5G during the uplink synchronization process. Synchronization signals are important part of a mobile communication process. In 5G, this type of signals are proposed and improved extensively to be able to cope with high latency and user capacity problems under channel fading, noise and interference stemming from other cells (See Chapter 2). When a user equipment (UE) boots itself up, it first tries to detect a surrounding base station and communicate with it for reporting its existence to the cell. Firstly this process starts with cell id identification and downlink synchronization signals. The main reason that the hand-shaking process

starts with downlink synchronization is that a base station can provide high transmit powers, hence it is fairly easier than the uplink synchronization process. Due to the challenging procedure requirements of the uplink process, some signal values should be known by UEs prior to uplink synchronization. These values are obtained via downlink processes [1], [10]. Usually, higher signal-to-noise ratios (SNRs) exist for the downlink case. However, in the uplink case, the antenna draws current from the cell phone battery, therefore it cannot use high output powers for synchronization signal transmission. Overall, SNRs for uplink cases are quite low compared to downlink cases.

Aforementioned challenges make the uplink synchronization process quite challenging. Without uplink synchronization, uplink data transfer cannot be successfully performed and more importantly, UE cannot be detected in the cell. Therefore, in 5G as well as in 4G, the uplink synchronization process aims to detect user equipment in the cell, and then determine possible time misalignment to completely match user equipment time schedule to base station's schedule [1], [10], [11]. Without this process, interference can occur and create destructive effects for data communication. Figure 1.1 shows possible interference scenarios [1]. It is noted that when there is no time alignment, UL (uplink) transmission and DL (downlink) reception occur at the same time in the user equipment. Therefore, it creates interference. Similarly, when there is uplink synchronization, reception of all UEs' uplink signal and transmission at the base station occurs at the same time. Additionally, in 5G as well as LTE, uplink orthogonality is maintained by ensuring that the transmissions from different UEs in a cell are time-aligned at the receiver of the base station. This avoids intra-cell interference occurring both among UEs assigned to transmit in consecutive subframes and among UEs transmitting on adjacent subcarriers [1].

Due to the preceding reasons, uplink synchronization and time alignment are crucial and very challenging problems. Based on an extensive literature search, it is noted that robust and easy to implement detectors are not available for the uplink synchronization process in 5G. It is also observed that the conventional detector does not use all the information available in the received signal, leading to a sub-optimal detection scheme (See Chapter 3). Based on these observations,

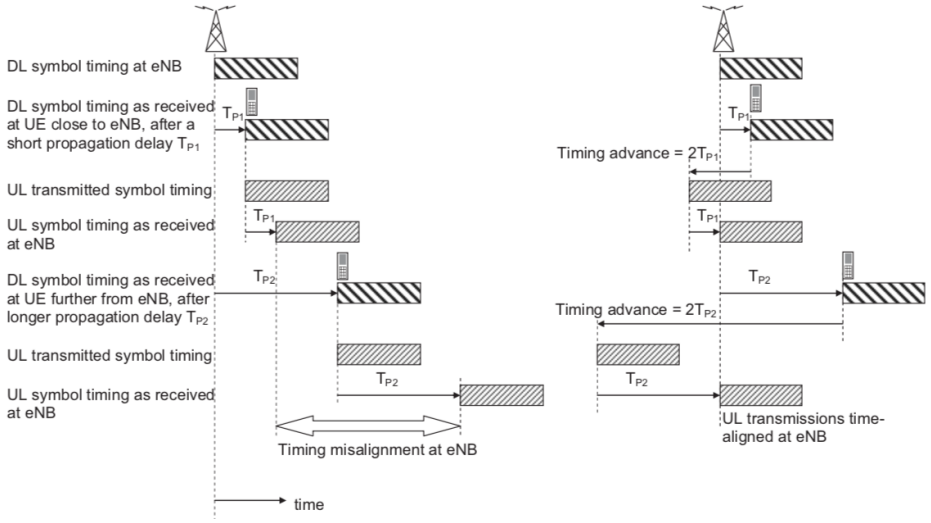

(a) without uplink synchronization (b) with uplink synchronization

Figure 1.1: Time alignment of uplink transmission [1].

this thesis aims to propose an improved detection approach that can outperform the conventional detector for the uplink process. By enhancing the robustness and performance, more UEs can be detected in the cell with reduced latency and interference. There is also another criterion for the proposed detector, since uplink synchronization is performed in the UE; namely, the power consumption of the detector is supposed to be as low as possible with the highest performance in order to meet the green 5G communication requirements mentioned in [8]. In addition, there are not any upper bounds on the detection performance related to uplink synchronization in the literature. In this thesis, such an upper bound is derived, which can be used to evaluate the performance of the conventional and proposed detectors.

1.2.2 Literature Review and Introduction to RACH Process

As the RACH process is an uplink process that occurs during initial access, SNRs are usually low and there is no channel state information (CSI) available at the receiver. Therefore, the RACH process is one of the most challenging and

complicated hand-shaking processes in LTE/5G as mentioned earlier. The RACH process starts when a UE boots up, or when a UE enters a new eNodeB radius. This process basically indicates which and how many UEs are inside the network and how far they operate from eNodeB [11]. As the uplink synchronization is performed by the RACH process, this hand-shaking process must be performed initially before sending any uplink information in the control channel.

In the physical layer, physical random access channel (PRACH) signals are created using Zaddoff-Chu (ZC) sequences which guarantee the ideal auto-correlation (zero cyclic auto-correlation) property among the ZC signals with the same root. Based on this property, we can detect the signals with the same root in the radius while rejecting the signals with different roots (i.e., those coming from other eNodeB zones). In 5G/LTE, 64 different preambles are defined for each format type [12]. Therefore, one eNodeB can serve only 64 different UEs at the same time. As a property of ZC sequences, the auto-correlation function shifts the peak that comes from the same root sequence by the amount of delay due to the distance of the UE from the cell center and, in addition, by the shift amount that is specified by the preamble index [13]. In order to detect and separate PRACH signals, all 64 preambles are cyclically shifted versions of each other. This is how a detector can detect and serve more than one signal by dividing the auto-correlation signal into 64 zones [1].

Normally, in the RACH process, it is expected to observe one peak in each zone of the auto-correlation signal. In 5G, the RACH process is not designed to serve multiple UEs with the same Cell Radio Network Temporary Identifier (C-RNTI). The case in which only one signal is detected in the zone is called the *contention free resolution*. However, there may be some cases in which multiple UEs randomly choose the same preamble index. This case is called *contention based detection* which is solved via a 4-step contention resolution method [11]. Due to the fact that distinguishing these two cases are hard to model, the conventional detector uses the same decision metric for contention free and contention based detection. That decision metric is the power delay profile (PDP) or equivalently, the energy of the signal. The main advantage of this metric is its low computational complexity. The conventional detector type uses a PDP based intuitive

solution for detecting PRACH signals [1]. There are also other types of detectors proposed in the literature. One of them is the forward consecutive mean excision (FCME) algorithm proposed in [14]. Similar to the conventional detector, FCME uses PDP; however, it performs an iterative technique to improve detection performance. The detector in [15] performs an iterative preamble reconstruction with interference cancellation. This method basically extracts signals with undesired roots by trial and error and minimizes the mean squared error (MSE) for the reference signal.

In this thesis, we investigate PRACH signal detection by modeling it as a binary hypothesis testing problem. Based on the hypothesis testing formulation, we propose a detector that employs zone based generalized likelihood ratio test (Z-GLRT) instead of point by point binary hypothesis testing, which is used in the conventional approach. The proposed detector is initially derived under the assumption that there can exist at most one PRACH signal in each zone. Also, a low-complexity version of the proposed detector is derived for practical implementations. In addition, the case with multiple PRACH signals in each zone is considered and the extension of the proposed detector is discussed. Moreover, we derive an ideal detector that provides an upper bound on detection performance, which can be used to evaluate performance of practical detection algorithms. Via extensive simulations, it is observed that the proposed approach outperforms the conventional detector in practical scenarios.

The remainder of the thesis is organized as follows: PRACH signal generation is explained in Chapter 2, and the conventional detector is discussed in Chapter 3. The proposed detectors, as well as an upper bound, are derived in Chapter 4. In Chapter 5, simulation results are presented, followed by the concluding remarks and future works in Chapter 6.

Chapter 2

PRACH Signal Generation

In this chapter, the PRACH signal generation is discussed. PRACH signals are determined as Zaddoff-Chu (ZC) sequences in 5G/LTE [12], [1]. The ZC sequence equation is as follows:

$$x_u(n) = e^{-j\frac{\pi un(n+1)}{N_{ZC}}}, \quad 0 \leq n \leq N_{ZC} - 1 \tag{2.1}$$

where n is the index, u is the root parameter, and N_{ZC} is the signal length. The reason for the selection of this sequence type is that the ZC sequences have a constant amplitude and the zero correlation property [16]. Namely, for all possible sequences, the signal power is one and the correlation of the same root has zero amplitude except for the location of the peak. The auto-correlation function of ZC sequences is given by

$$c_{uu} = \sum_{n=0}^{N_{ZC}-1} a_u(n) a_u^*(n + \tau + C_l) = \delta(\tau + C_l) \tag{2.2}$$

where C_l is the cyclic shift amount and τ is the amount of delay that can be nonzero depending on the channel delay or UE's position. All values in (2.2) are zero except for the place at which the peak occurs as shown in Figure 2.1. In general, the position of the peak can be anywhere depending on channel/propagation delays. Additionally, the position of the peak informs the UE about how much delay occurs in the medium so that it can adjust itself accordingly. The peak

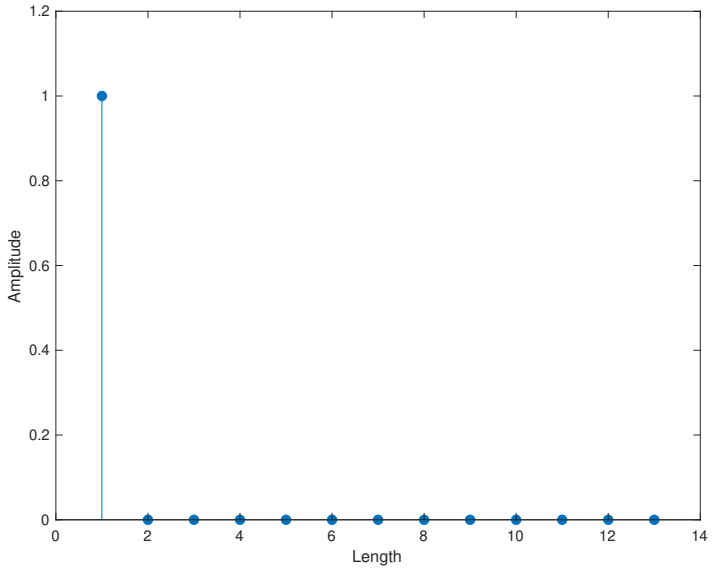

Figure 2.1: Correlation signal with one peak in the zone under no noise and channel delay.

at C_l occurs only when the ZC sequence is correlated with another ZC sequence with the same root. (The peak in the signal occurs at index C_l provided that there is no delay from the channel or due to UE's position.) If two ZC sequences have different roots, then their cross-correlation function has a constant value of $1/\sqrt{N_{\text{ZC}}}$, which gets closer to zero as the ZC signal gets longer [17], [18], [19], [20].

In order to assign an identity to each UE in 5G/LTE, the C_l parameter is used along with a parameter called the zero correlation zone, N_{CS}. The N_{CS} parameter separates each signal into 64 zones. Therefore, eNodeB can differentiate a UE from another UE as the preamble index (which contains a predetermined cyclic shift amount) is different for each of them. The formulation of C_l is given as follows:

$$C_l = lN_{CS}\,,\ l = 0, 1, \ldots, \left\lfloor \frac{N_{ZC}}{N_{CS}} \right\rfloor - 1 \tag{2.3}$$

where N_{CS} value is different for all cells depending on the cell size [21]. In larger cells, as the user position can be far from the center, a larger delay can occur in the received signal; hence, a larger N_{CS} is required. However, a larger N_{CS}

decreases the zone number for one root sequence, thus, in that case, multiple rooted ZC sequences are used to obtain the preamble number of 64 [12].

In 5G standards in [12], two different ZC sequence lengths are accepted, which correspond to long and short preambles. The long preamble has a signal length of 839 while the short preamble has a length of 139. Therefore, if we have 64 different zones and if we use long preambles by using one root sequence, then we need to have a maximum value of 13 as the length of the zero correlation zone since $\lfloor \frac{839}{64} \rfloor = 13$. The decision of choosing long or short preambles depends on the cell radius. If the cell radius is large (small), then long (short) preambles are chosen.

In order to detect PRACH signals, all detector types should have a threshold value to compare the noise only hypothesis ($\mathcal{H}_0$) against the signal plus noise hypothesis ($\mathcal{H}_1$). Normally, in 5G/LTE, only one signal is expected in each zone for a rapid synchronization process. If a single PRACH signal is detected in a zone, then gNodeB chooses $\mathcal{H}_1$ and responds to this with an ID and follow-up data. On the contrary, suppose that there exist more than one UEs in a zone. Then, three case can occur. First, none of the UEs receives or detects the gNodeB message. Then, all UEs again search for gNodeB by increasing the power of the transmitted PRACH signal. Second, only one of the UEs receives the response message (random access response (RAR)), and the rest repeat the PRACH signal with more power. Lastly, more than one UEs get the response and the UE that detects its own identity in the response, transmits another response (HARQ feedback) indicating that it has detected and understood the response from the network. With the help of this signal, other UEs understand that there was a collision. As a result, they do not respond and start the RACH process all over again [11], [22], [23]. This type of resolution of PRACH signals is called the contention based resolution, which is followed by a 4-step resolution procedure. This case, as expected, increases the latency. (There are some proposals about a 2-step RACH approach that reduces all of the back and forth response signaling by employing only two-step signaling for both contention resolution and contention free RACH process [24], [25].)

Chapter 3

Conventional Detector

It is complex to handle the contention based and contention free resolutions via (near) optimal detectors. Therefore, the conventional detector uses signal energy or PDP to decide whether there exists a peak or not. The correlation operation and PDP can be expressed as follows:

$$r_i = \sum_{n=0}^{N_{ZC}-1} y(n)x^*((n+i)_{N_{ZC}}) \tag{3.1}$$

$$PDP(i) = |r_i|^2 \underset{H_0}{\overset{H_1}{\gtrless}} T_{con} \tag{3.2}$$

where r_i is the correlation signal, y is the received signal, x is the reference preamble, and T_{con} is the threshold for the conventional detector. Namely, the energy of the correlation signal is compared against a threshold to determine the absence ($\mathcal{H}_0$) or presence ($\mathcal{H}_1$) of a peak (user) at a given index i, where $i \in \{0, 1, \ldots, N_{ZC} - 1\}$.

In [1], the threshold setting is performed by sending no signals (i.e., noise only) to the detector and determining the noise floor and the threshold for a desired value for the false alarm probability, P_{fa}. This process is commonly implemented offline. Another method for threshold setting is to use of the sample variance of the received signal, which is also an offline process. The formulation for setting

the threshold via this method is given by

$$T_{con} = \frac{\epsilon}{(N_{ZC}-1)} \sum_{n=0}^{N_{ZC}-1} |y(n)|^2 \tag{3.3}$$

where ϵ is a constant number that is found by Monte Carlo trials. Parameter ϵ is used to adjust the threshold value corresponding to a desired P_{fa} under a given SNR value so that P_{fa} can be kept at similar levels for different SNRs. The main drawback of this method is that in the received signal, there may be multiple PRACH signals in addition to noise. Therefore, in crowded cells, the variance level, hence T_{con}, can increase, which can result in dramatically decreased values of P_{fa}. In addition, ϵ is valid only for a fixed SNR value, and if the SNR changes drastically, then ϵ can get unsuitable for the specific value of P_{fa}. If the SNR versus the threshold relation were linear, the ϵ parameter could keep the false alarm probability the same for all SNRs. However, the noise level cannot be known exactly in practice; therefore, estimating the noise level is an important step. The threshold setting approach in (3.3) basically employs the sample variance to estimate the noise level in the system. Therefore, under low arrival rates, it can set the false alarm probability close to a desired level. However, under high arrival rates, the sample variance can significantly be affected by presence of signals and can cause the false alarm probability to be set to incorrect levels.

Remark 1: It should be noted that the conventional detector in (3.2) performs hypothesis testing for each index of the correlation signal. We can call this approach *point by point hypothesis testing*. As discussed in the next chapter, using the whole correlation signal at once (instead of performing a point by point test) can lead to improved performance.

Remark 2: It can be shown that the conventional detector in (3.2) can be regarded as a point by point GLRT under certain conditions when the noise variance is assumed to be known. To this end, the correlation signal at the ith index, r_i in (3.1), is modeled as a circularly symmetric complex Gaussian random variable $CN(0,\sigma^2)$ or $CN(A,\sigma^2)$ under $\mathcal{H}_0$ and $\mathcal{H}_1$, respectively, where σ^2 is the known noise variance and A represents the (complex) signal component [26]. In

particular, the correlation signal at the ith index is distributed as follows:

$$\mathcal{H}_0 \ : \ p(r_i|\mathcal{H}_0) = \frac{1}{\pi\sigma^2} e^{-\frac{|r_i|^2}{\sigma^2}} \tag{3.4}$$

$$\mathcal{H}_1 \ : \ p(r_i|\mathcal{H}_1) = \frac{1}{\pi\sigma^2} e^{-\frac{|r_i-A|^2}{\sigma^2}} \tag{3.5}$$

Based on this model, the GLRT is obtained as follows:

$$L(r_i) = \frac{\max\limits_{A} \frac{1}{\pi\sigma^2} e^{-\frac{|r_i-A|^2}{\sigma^2}}}{\frac{1}{\pi\sigma^2} e^{-\frac{|r_i|^2}{\sigma^2}}} \underset{\mathcal{H}_0}{\overset{\mathcal{H}_1}{\gtrless}} \tau \tag{3.6}$$

$$\implies |r_i|^2 \underset{\mathcal{H}_0}{\overset{\mathcal{H}_1}{\gtrless}} \tau' \tag{3.7}$$

Hence, performing a GLRT for each point (index) of the correlation signal corresponds to the conventional detector under the assumption of a known noise variance (cf. (3.2) and (3.7)). Therefore, using the energy of the correlation signal as a decision metric is a reasonable way to detect PRACH signals. However, as mentioned in Remark 1, point by point hypothesis testing is not optimal in general.

Remark 3: In order to determine the presence of a PRACH signal in a given zone, the conventional approach can compare the maximum energy in that zone against a threshold. In other words, a PRACH signal is declared to exist in a zone if at least one signal energy is above the threshold.

Chapter 4

Proposed Detectors Based on Zone Based GLRT

4.1 Zone based GLRT (Z-GLRT)

The main idea behind the proposed approach is to perform PRACH signal detection zone by zone instead of point by point as in Chapter 3. To this aim, a binary hypothesis testing problem is formulated to determine whether there exists a signal in a given zone. As discussed in Chapter 2, each correlation signal is divided into 64 zones, which are called zero correlation zones, and the length of the zones are determined by parameter N_{CS}. The detection approaches developed for a given zone in this chapter are to be applied for each zone (i.e., 64 different zones for LTE/5G) to detect possible PRACH signals in the whole received signal.

First, we consider the case in which there exists at most one PRACH signal in each zone. In this case, if there exists a UE PRACH signal in a given zone, we expect to see a peak inside that zone due to the PRACH signal. Since the exact location of a peak is unknown and there is no prior information about it in general, it is assumed that the location of a peak is uniformly distributed in each zone. This assumption is reasonable since the location of a peak inside

a zone changes due to the propagation delay which depends on UE's position with respect to eNodeB and any additional channel delays. (For example, in the absence of any delays, the peak is observed at the first index of the correlation signal.)

Let N denote the length of a zone and $r_1, \ldots, r_N$ represent the samples of the correlation signal in a zone.[1] Under the described setting, the likelihood function in the absence of a PRACH signal can be expressed as follows:

$$p(r_1, r_2, \ldots, r_N|\mathcal{H}_0) = \frac{1}{(\pi\sigma^2)^N} e^{-\frac{1}{\sigma^2}\sum_{i=1}^{N}|r_i|^2} \tag{4.1}$$

where $\mathcal{H}_0$ represents the noise only hypothesis. In deriving (4.1), it is assumed that the noise components are modeled as independent and identically distributed circularly symmetric complex Gaussian random variables with variance σ^2 [26]. Similarly, the likelihood function in the presence of a PRACH signal ($\mathcal{H}_1$) can be formulated as

$$p(r_1, r_2, \ldots, r_N|\mathcal{H}_1) = \frac{1}{N}\sum_{k=1}^{N} \frac{1}{(\pi\sigma^2)^N} e^{-\frac{|r_k - A|^2}{\sigma^2}} \prod_{i=1, i\neq k}^{N} e^{-\frac{|r_i|^2}{\sigma^2}} \tag{4.2}$$

where A is related to the peak value and k is the index that represents the location of the peak, which is modeled as a uniform random variable.

In practical scenarios, the values of σ^2 and A in (4.1) and (4.2) are unknown. Therefore, we propose a GLRT approach as follows:

$$\frac{\max\limits_{\sigma^2, A} p(r_1, \ldots, r_N|\mathcal{H}_1)}{\max\limits_{\sigma^2} p(r_1, \ldots, r_N|\mathcal{H}_0)} \underset{\mathcal{H}_0}{\overset{\mathcal{H}_1}{\gtrless}} \tau_Z \tag{4.3}$$

where τ_Z is the threshold for zone based GLRT (Z-GLRT). Namely, the maximum likelihood estimates (MLEs) of the unknown parameters are calculated under each hypothesis and then a likelihood ratio test (LRT) is performed [27, 28].

The value of σ^2 that maximizes (4.1) can be obtained as

$$\widehat{\sigma}_0^2 = \underset{\sigma^2}{\text{argmax}} \frac{1}{(\pi\sigma^2)^N} e^{-\frac{1}{\sigma^2}\sum_{i=1}^{N}|r_i|^2} = \frac{1}{N}\sum_{i=1}^{N}|r_i|^2 \tag{4.4}$$

[1]For compactness of notation, $r_1, \ldots, r_N$ are used to represent the samples in *any* zone without employing distinct indices for different zones.

On the other hand, the values of σ^2 and A that maximize (4.2) cannot be obtained in closed forms. Therefore, numerical evaluation is required to obtain the MLEs for σ^2 and A under $\mathcal{H}_1$. Let $\widehat{\sigma}_1^2$ and $\widehat{A}$ denote these MLEs; that is,

$$\left(\widehat{\sigma}_1^2, \widehat{A}\right) = \underset{\sigma^2, A}{\operatorname{argmax}} \sum_{k=1}^{N} \sigma^{-2N} e^{-\frac{|r_k - A|^2}{\sigma^2}} \prod_{i=1, i\neq k}^{N} e^{-\frac{|r_i|^2}{\sigma^2}} \tag{4.5}$$

where the constant terms in (4.2) are omitted. In the numerical examples, we assign certain intervals for σ^2 and A and perform exhaustive search over those intervals. (Another approach with lower computational complexity is proposed below.)

Based on (4.4) and (4.5), Z-GLRT in (4.3) can be expressed, after some manipulation, as

$$\left(\frac{\widehat{\sigma}_0}{\widehat{\sigma}_1}\right)^{2N} \sum_{k=1}^{N} e^{-\frac{|r_k - \widehat{A}|^2}{\widehat{\sigma}_1^2}} \prod_{i=1, i\neq k}^{N} e^{-\frac{|r_i|^2}{\widehat{\sigma}_1^2}} \underset{H_0}{\overset{H_1}{\gtrless}} \tau_Z' \tag{4.6}$$

where $\tau_Z' = Ne^{-N}\tau_Z$.

It should be noted that Z-GLRT in (4.6) is designed for one zone. Therefore, this detector can be executed for each of the 64 zones in order to decide for the absence or presence of PRACH signals in each zone.

4.2 Zone based GLRT with Low Complexity

Since it is required to perform a search over a three-dimensional parameter space to specify $\widehat{\sigma}_1^2$ and $\widehat{A}$ (i.e., $Re\{\widehat{A}\}$ and $Im\{\widehat{A}\}$) in (4.6) (see (4.5)), the computational complexity of Z-GLRT is high in general. In order to propose a low complexity alternative, consider a two-step approach in which the value of σ^2 under $\mathcal{H}_1$ is estimated in the first step as follows. Suppose that the location of the peak is known under $\mathcal{H}_1$ and the likelihood function is given by (cf. (4.2))

$$p(r_1, r_2, \ldots, r_N|\mathcal{H}_1) = \frac{1}{(\pi\sigma^2)^N} e^{-\frac{|r_m - A|^2}{\sigma^2}} \prod_{i=1, i\neq m}^{N} e^{-\frac{|r_i|^2}{\sigma^2}} \tag{4.7}$$

where m is the *known* index for the peak. In this scenario, the MLE for σ^2 can be obtained from (4.7) as (please see Appendix A)

$$\tilde{\sigma}_1^2 = \frac{1}{N} \sum_{i=1, i \neq m}^{N} |r_i|^2 . \tag{4.8}$$

Since the location of the peak is not known in practice, it is estimated as

$$m = \underset{i \in \{1,\ldots,N\}}{\operatorname{argmax}} |r_i|^2 . \tag{4.9}$$

That is, the sample with the maximum magnitude is considered as the peak. If it is known that there can exist at most one peak in the whole subframe, i.e., in the 64 zones, then the estimate in (4.8) can be updated as

$$\tilde{\sigma}_1^2 = \frac{1}{L} \sum_{i=1, i \neq m}^{L} |r_i|^2 \tag{4.10}$$

where L is the number of samples in the subframe (e.g., $L = 64N$) and $m = \operatorname{argmax}_{i \in \{1,\ldots,L\}} |r_i|^2$.

In the second step, the following zone based GLRT, called *simplified zone based GLRT (SZ-GLRT)*, is proposed:

$$\left(\frac{\widehat{\sigma}_0}{\tilde{\sigma}_1} \right)^{2N} \sum_{k=1}^{N} e^{-\frac{|r_k - \tilde{A}|^2}{\tilde{\sigma}_1^2}} \prod_{i=1, i \neq k}^{N} e^{-\frac{|r_i|^2}{\tilde{\sigma}_1^2}} \underset{\mathcal{H}_0}{\overset{\mathcal{H}_1}{\gtrless}} \tau_{SZ} \tag{4.11}$$

where τ_{SZ} is the threshold for SZ-GLRT, $\widehat{\sigma}_0^2$ is given by (4.4), $\tilde{\sigma}_1^2$ is as in (4.8) or (4.10), and $\tilde{A}$ is obtained as (cf. (4.5))

$$\tilde{A} = \underset{A}{\operatorname{argmax}} \sum_{k=1}^{N} \tilde{\sigma}_1^{-2N} e^{-\frac{|r_k - A|^2}{\tilde{\sigma}_1^2}} \prod_{i=1, i \neq k}^{N} e^{-\frac{|r_i|^2}{\tilde{\sigma}_1^2}} \tag{4.12}$$

The main idea behind SZ-GLRT is to employ the intuitive (ad-hoc) estimate for σ^2 under $\mathcal{H}_1$ in (4.8) or (4.10) in the Z-GLRT in (4.6). It is noted that SZ-GLRT in (4.11) has lower computational complexity than Z-GLRT in (4.6) since a two-dimensional search is required in the former (see (4.12)) instead of a three-dimensional search.

4.3 Scenario with Multiple PRACH Signals in a Zone

In sections 4.1 and 4.2, it is assumed that there exists at most one PRACH signal in each zone. In this section, we consider the scenario in which there can exist multiple PRACH signals in a zone. This scenario is classified as collision and can only be resolved via the 4-step contention based resolution [1]. Even though this case is undesirable, it can be necessary to detect the presence of PRACH signals in this case, as well.

Before explaining the collision case, it should be emphasized that in 5G/LTE standards, PRACH signals are not allowed to be sent anytime or in any random subframe. Before the RACH process, by using control channels, eNodeB provides the required subframe indices and the ZC sequence root to UE in the Radio Resource Controller (RRC) [22]. For instance, in busy network cases, eNodeB could say that UE can transmit PRACH signals in any subframe for a period of time until the busy schedule is completed. After this process, eNodeB could also say that UE can only be allowed to transmit a PRACH signal once in 16 frames, which corresponds to a period of 16 ms. In other words, eNodeB adjusts this process according to the arrival rate.

The probability of having more than one PRACH signals in a one zone (i.e., collision probability) can be calculated as $1 - 63!(64)^{n-1}/(63-n)!$, where n is the number of users in the subframe. The probability of collision versus number of UEis given in 4.1. For example, if 10 users exist in the system in a 1 ms time slot, then the collision probability is approximately equal to 0.5, which is quite high. However, having 10 users in every 1 ms time slot corresponds to 10000 users in 1 second. In other words, in order to reach a 10 user mean in the RACH process, 10000 users should boot up their equipment or come to the cell in one second, which seems unlikely in real life even if eNodeB operates in very busy conditions. Still, there may be places such as concert halls, stadiums, and large meeting areas, where the mean user arrival rate can be sufficiently high so that the collision probability is non-negligible and there can exist more than one PRACH

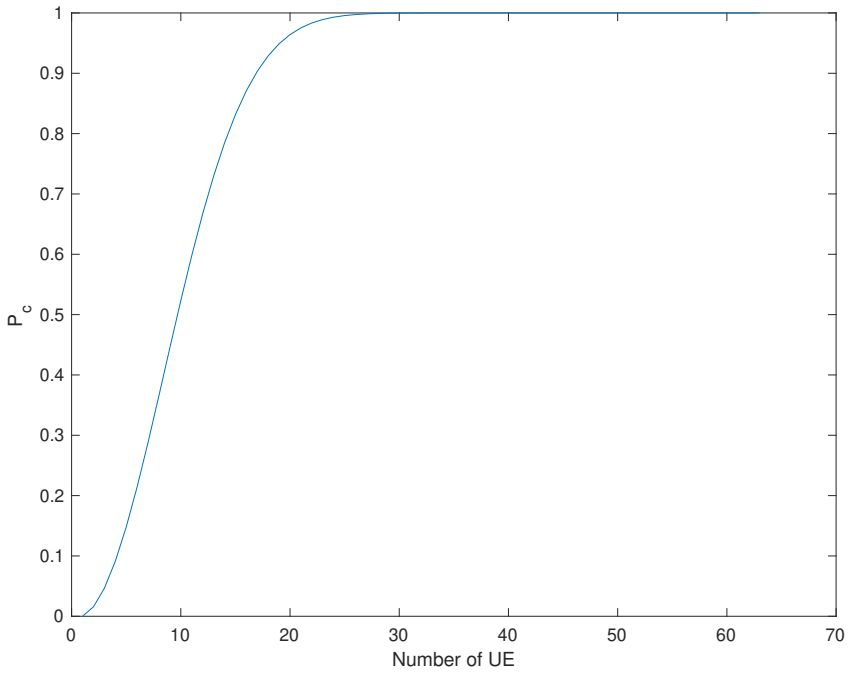

Figure 4.1: Probability of collision in a zone.

signals in some zones.

The following observations can be extracted from Figure 4.1. In order to cover multiple peak cases, we can extend our proposed zone based GLRT detector. Additionally, even if P_c is high, many of the zones in the signal can have no or only one peak. With the increase of the UE number, many zones start to have multiple peaks rather than no peak or only one peak. Therefore, the model in equation (4.2) starts to perform worse as it assumes only one peak in the zone. Yet, for practical reasons,, we can still use the proposed detector, even though it does not have the correct model for many zones.

To cover the scenario in which there can exist multiple PRACH signals in a given zone, the hypotheses are defined as no PRACH signals in the zone ($\mathcal{H}_0$) and at least one PRACH signal in the zone ($\mathcal{H}_1$). Since the $\mathcal{H}_0$ hypothesis is the same as the previous scenario, the likelihood function under $\mathcal{H}_0$ is again given by

(4.1). On the other hand, the likelihood function under $\mathcal{H}_1$ is obtained as follows:

$$p(r_1, r_2, \ldots, r_N|\mathcal{H}_1) = \frac{1}{N^M(\pi\sigma^2)^N} \sum_{k_1=1}^{N} \cdots \sum_{k_M=1}^{N} e^{-\frac{1}{\sigma^2}\left(\sum_{v=1}^{M}|r_{k_v}-A_v|^2+\sum_{i=1,i\neq k_1,\ldots,k_M}^{N}|r_i|^2\right)} \tag{4.13}$$

where M is the maximum number of PRACH signals that can be observed in the zone, k_v, $v \in \{1, \ldots, M\}$ is the index of each PRACH signal in the zone, and A_v is the complex amplitude due to the vth PRACH signal. If the maximum number of PRACH signals, M, cannot be determined in advance, it can be taken as N since it corresponds to the most generic scenario as A_v's can also be set to zero.

Under the described setting, zone based GLRT in the presence of multiple PRACH signals can be formulated as

$$\frac{\max\limits_{\sigma^2, A_1, \ldots, A_M} p(r_1, \ldots, r_N|\mathcal{H}_1)}{(\widehat{\sigma}_0^2)^{-N}} \underset{\mathcal{H}_0}{\overset{\mathcal{H}_1}{\gtrless}} \tau_{ZM} \tag{4.14}$$

where τ_{ZM} is the threshold, $\widehat{\sigma}_0^2$ is given by (4.4) and $p(r_1, \ldots, r_N|\mathcal{H}_1)$ is as in (4.13).

The GLRT in (4.14) has very high computational complexity; hence, may not be employed in practice. Therefore, we propose a low-complexity approach, which only requires the knowledge of the expected number of users in a subframe. Let κ denote the expected (average) number of users in a subframe. Then, it can be shown that a reasonable estimator (please see Appendix B for justification) for σ^2 under $\mathcal{H}_1$ is given by

$$\bar{\sigma}_1^2 = \frac{1}{L} \sum_{i=1,\, i\notin M_\kappa}^{L} |r_i|^2 \tag{4.15}$$

where L is the number of samples in the subframe and M_κ is the set of indices corresponding to the largest κ correlation values, that is, M_κ is a subset of $\{1, \ldots, L\}$ such that $|M_\kappa| = \kappa$ and $|r_i|^2 \geq |r_j|^2 \; \forall\, i \in M_\kappa \;\&\; j \notin M_\kappa$. Then, to obtain a low-complexity detector, only the most significant peak is considered and the rest are modeled as noise components. That is, the single peak model in section 4.1 is adopted. Then, the following zone based GLRT, called *simplified zone based*

GLRT for multiple peaks (SZ-GLRT-M), is proposed:

$$\left(\frac{\widehat{\sigma}_0}{\bar{\sigma}_1}\right)^{2N} \sum_{k=1}^{N} e^{-\frac{|r_k-\bar{A}|^2}{\bar{\sigma}_1^2}} \prod_{i=1,i\neq k}^{N} e^{-\frac{|r_i|^2}{\bar{\sigma}_1^2}} \underset{\mathcal{H}_0}{\overset{\mathcal{H}_1}{\gtrless}} \tau_{SZM} \tag{4.16}$$

where τ_{SZM} is the threshold for SZ-GLRT-M, $\widehat{\sigma}_0^2$ is given by (4.4), $\bar{\sigma}_1^2$ is as in (4.15), and $\bar{A}$ is obtained as (cf. (4.5))

$$\bar{A} = \underset{A}{\operatorname{argmax}} \sum_{k=1}^{N} \bar{\sigma}_1^{-2N} e^{-\frac{|r_k-A|^2}{\bar{\sigma}_1^2}} \prod_{i=1,i\neq k}^{N} e^{-\frac{|r_i|^2}{\bar{\sigma}_1^2}} \tag{4.17}$$

The main motivation behind SZ-GLRT-M is to utilize a low-complexity detector by assuming the single peak model in section 4.1 (see (4.6)) and employing the ad-hoc estimate in (4.15) for σ^2 under $\mathcal{H}_1$. In this manner, instead of performing a search over a $(2M+1)$ dimensional space (see (4.14)), SZ-GLRT-M performs a search over a two-dimensional space (see (4.17)) for PRACH signal detection.

4.4 Upper Bound for PRACH Detection

To derive an ideal detector that provides an upper bound on detection performance, suppose that the unknown parameters in (4.1) and (4.13), namely, the variance and the amplitudes, are known. Then, based on (4.1) and (4.13), the LRT can be formed and simplified as follows:

$$\frac{\frac{1}{N^M(\pi\sigma^2)^N} \sum_{k_1=1}^{N} \cdots \sum_{k_M=1}^{N} e^{-\frac{1}{\sigma^2}\left(\sum_{v=1}^{M} |r_{k_v}-A_v|^2 + \sum_{i=1,i\neq k_1,\ldots,k_M}^{N} |r_i|^2\right)}}{\frac{1}{(\pi\sigma^2)^N} e^{-\frac{1}{\sigma^2}\sum_{i=1}^{N}|r_i|^2}} \underset{\mathcal{H}_0}{\overset{\mathcal{H}_1}{\gtrless}} \tau \tag{4.18}$$

$$\Longrightarrow \frac{1}{N^M} \sum_{k_1=1}^{N} \cdots \sum_{k_M=1}^{N} e^{-\frac{1}{\sigma^2}\sum_{v=1}^{M}(|r_{k_v}-A_v|^2-|r_{k_v}|^2)} \underset{\mathcal{H}_0}{\overset{\mathcal{H}_1}{\gtrless}} \tau \tag{4.19}$$

$$\Longrightarrow \frac{1}{N^M} \sum_{k_1=1}^{N} \cdots \sum_{k_M=1}^{N} e^{-\frac{1}{\sigma^2}\sum_{v=1}^{M}(|A_v|^2-2Re\{A_v^* r_{k_v}\})} \underset{\mathcal{H}_0}{\overset{\mathcal{H}_1}{\gtrless}} \tau \tag{4.20}$$

$$\Longrightarrow \sum_{k_1=1}^{N} \cdots \sum_{k_M=1}^{N} e^{\frac{2}{\sigma^2}\sum_{v=1}^{M} Re\{A_v^* r_{k_v}\}} \underset{\mathcal{H}_0}{\overset{\mathcal{H}_1}{\gtrless}} \tau_{up} \tag{4.21}$$

where $\tau_{up} = \tau\, N^M e^{\frac{1}{\sigma^2}\sum_{v=1}^{M}|A_v|^2}$ is the threshold of the ideal detector employed for deriving the upper bound. Since the detector in (4.21) is designed under

the assumption of known variance and peak values, its detection performance provides a performance upper bound for practical estimators, as investigated in the next chapter.

If there exists only one peak in the zone, then the detector in (4.21) reduces to following form:

$$\sum_{k=1}^{N} e^{\frac{2}{\sigma^2} Re\{A^* r_k\}} \underset{\mathcal{H}_0}{\overset{\mathcal{H}_1}{\gtrless}} \tau_{up} \tag{4.22}$$

where A is the peak related value.

Chapter 5

Simulation Results

In this chapter, simulation results are presented to investigate the performance of the proposed approach. In the simulations, format 0 preamble signal, which has the shortest zone length, is used as other long preamble formats are very similar to this particular format [1], [21]. Since improved performance results are expected for longer zones, simulations are performed for the shortest possible zone in order to observe the performance of the proposed approach in a worst-case scenario. In presenting the simulation results, we will first consider the AWGN channel model and then use the TDL-C channel model (with 30 ns delay spread and 5 Hz Doppler spread) for more realistic simulations [29], [30], [31].

In the first scenario, it is assumed that at most one peak can occur in a subframe. Also, the correlation signal consists of 64 zones, each zone has 13 samples, and the peak in the signal (if it exists) is assigned randomly to one of the zones. Figures 5.1–5.3 below are obtained based on the first scenario.

In Figure 5.1, the ROC curves are presented for the proposed detectors (Z-GLRT and SZ-GLRT), the conventional detector (see Remark 3), and the upper bound in the presence of an AWGN channel. In implementing SZ-GLRT, the decision rule in (4.11) is used together with (4.10) due to the assumption that

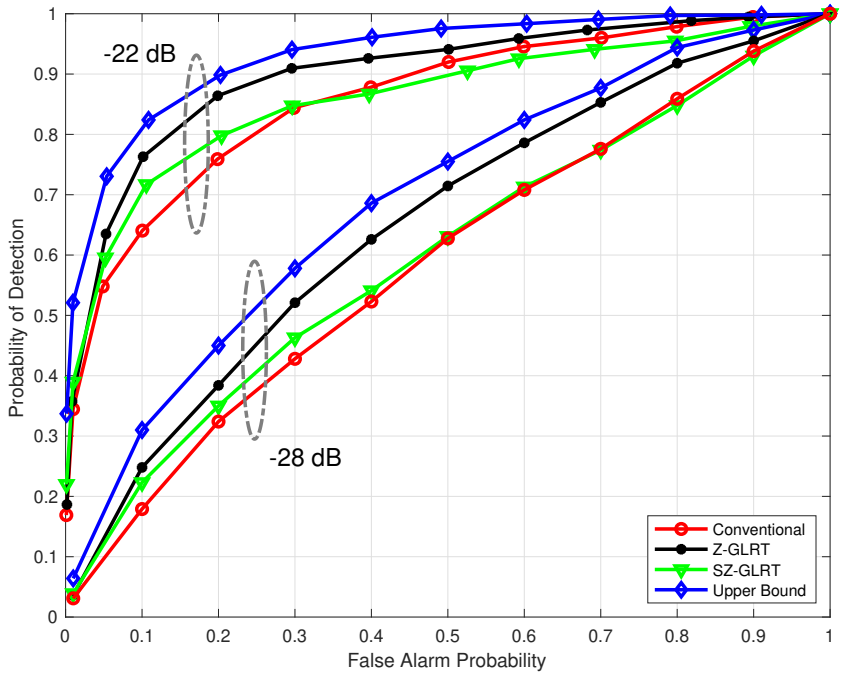

Figure 5.1: ROCs curve at SNR $= -28\,\mathrm{dB}$ and SNR $= -22\,\mathrm{dB}$ under AWGN channel.

at most one peak can occur in a subframe in the considered scenario. From Figure 5.1, it is observed that Z-GLRT always performs better than the conventional detector and its performance is close to the upper bound. On the other hand, SZ-GLRT achieves higher detection probabilities than the conventional detector (and Z-GLRT) in the region of (very) low false alarm probabilities. For higher values of the false alarm probability, SZ-GLRT performs worse than both the conventional detector and Z-GLRT. Since SZ-GLRT uses an ad-hoc estimator for the noise variance, it does not provide consistent improvements over the conventional detector. However, it is observed to be a desirable alternative for low false alarm probabilities, which are the main target in common real-life scenarios. The performance gap between SZ-GLRT and the conventional detector depends on both the SNR and the false alarm probability. In particular, SZ-GLRT has better performance at low false alarm probabilities and low-to-medium SNR values. This can be seen more clearly in Figure 5.2, which illustrates the detection probability versus SNR curves in the presence of an AWGN channel. In this figure, SZ-GLRT is always better than the conventional detector and the performance gap between the two detectors is more distinct at low-to-medium SNR values. Moreover, it is noted that Z-GLRT always achieves higher detection probabilities than than the conventional detector; however, it is outperformed by SZ-GLRT at low-to-medium SNRs.

In Figure 5.3, the ROC curves are presented for the proposed detectors, the conventional detector, and the upper bound in the presence of the TDL-C channel for an SNR of $-22\,\mathrm{dB}$. As in the case of the AWGN channel, Z-GLRT achieves higher detection probabilities than the conventional detector for all false alarm probabilities. Compared to the results for the AWGN channel at $\mathrm{SNR} = -22\,\mathrm{dB}$, the performance of all the detectors reduces under the TDL-C channel, as expected. Also, SZ-GLRT is again better at low false alarm probabilities than both Z-GLRT and the conventional detector; however, it performs worse than the others as the false alarm probability increases. Overall, the performance trends are very similar in the AWGN and TDL-C channel scenarios.

In the second scenario, the arrival of users to the cell is modeled by a Poisson distribution with a mean value of κ in the interval of a subframe. Also, κ is

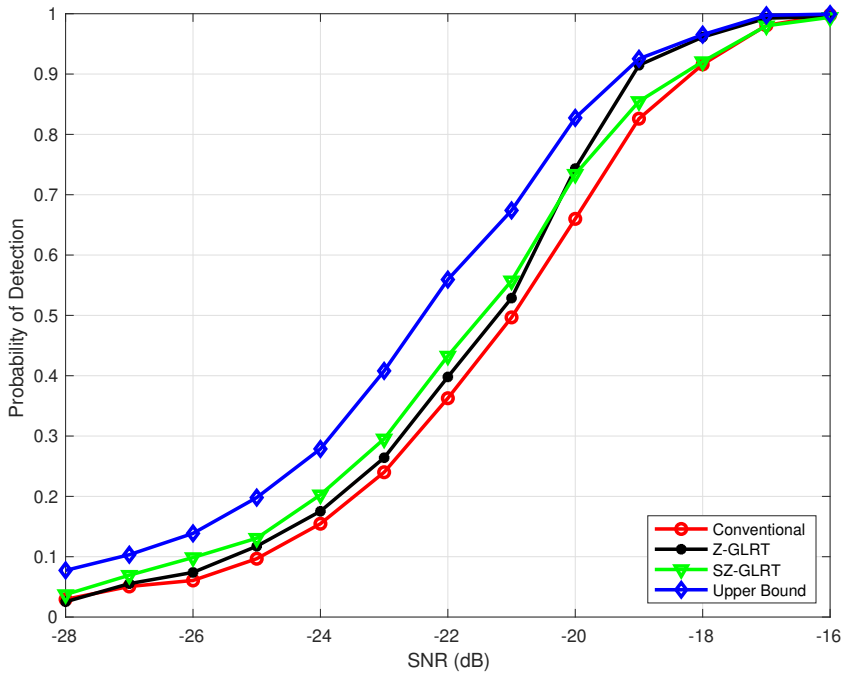

Figure 5.2: Detection probability versus SNR under AWGN channel for $P_{fa} = 10^{-2}$.

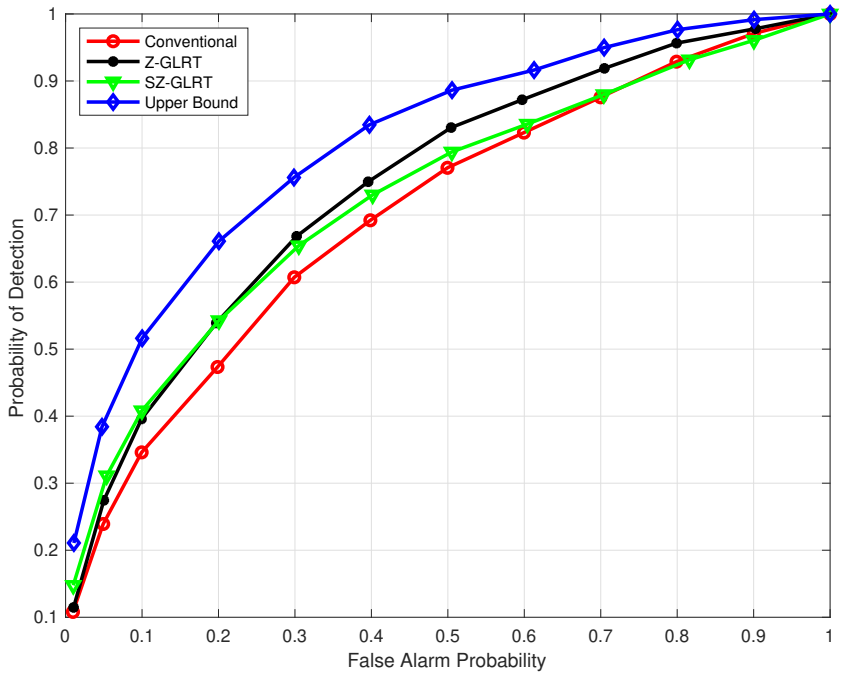

Figure 5.3: ROC curves at SNR $= -22$ dB under TDL-C channel.

set to 1 and the duration of each subframe is 1 ms. These values are selected due to their practicality, which are also specified as such in [32]. In Figure 5.4, the ROC curves are provided for the SZ-GLRT-M detector, the conventional detector, and the upper bound in the presence of the TDL-C channel. Similar results to those in Figures 5.1 and 5.3 are observed. Namely, SZ-GLRT-M achieves higher detection probabilities than the conventional detector for practical values of the false alarm probability. However, the performance gap decreases as the false alarm probability increases. In addition, when the performance of the SZ-GLRT detector in Figure 5.3 is compared to that of the SZ-GLRT-M detector in Figure 5.4, it is noted that SZ-GLRT-M performs slightly worse than SZ-GLRT at high false alarm probabilities. This is due to the fact that there can exist multiple PRACH signals in the second scenario. Although both SZ-GLRT and SZ-GLRT-M are derived under the assumption of at most one PRACH signal in each zone, it is possible that there exist multiple signals in a zone for the scenario in Figure 5.4. Therefore, performance degradation is observed due to the mismatch between the assumed and the actual models.

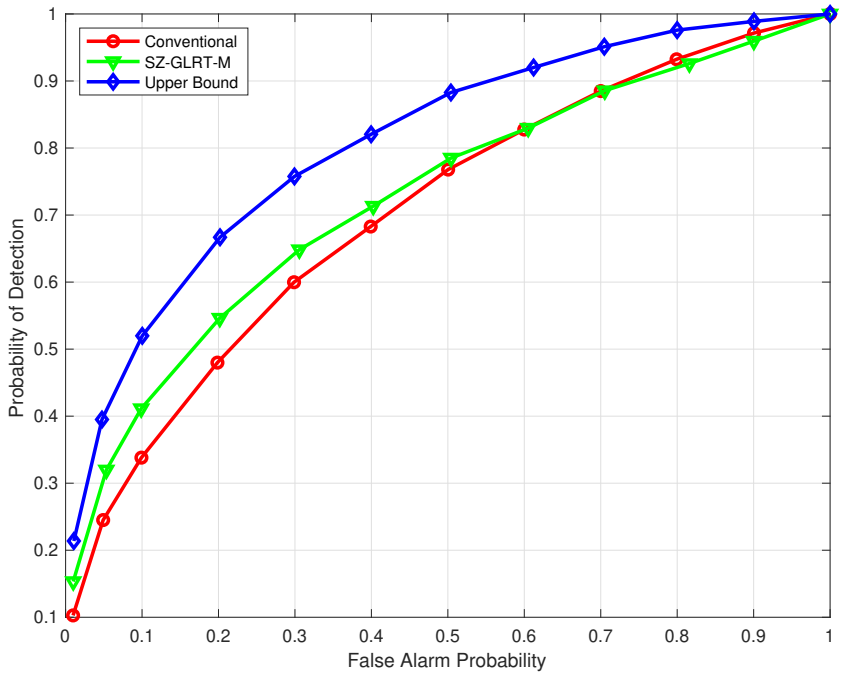

Figure 5.4: ROC curves at SNR $= -22\,\mathrm{dB}$ under TDL-C channel with $\kappa = 1$.

Since SZ-GLRT-M is derived under the assumption that there can exist at most one PRACH signal in each zone, its performance is expected to degrade with κ (as the probability of having more than one PRACH signal in a zone increases with κ). To determine the value of κ after which the conventional detector starts having higher detection probabilities than SZ-GLRT-M, the detection probability is plotted versus κ for two different false alarm probabilities and SNRs in Figures 5.5 and 5.6. It is observed that around $\kappa = 60$ at $P_{fa} = 10^{-1}$ and around $\kappa = 80$ at $P_{fa} = 10^{-2}$, SZ-GLRT-M is outperformed by the conventional detector for the case of SNR $= -22\,\mathrm{dB}$ (Figure 5.5). Such high mean arrival rates (κ's) are not expected in practical applications since they correspond to 6×10^4 and 8×10^4 mean arrivals of UEs in one second. In Figure 5.5, the detection performance of the conventional detector increases with κ. This is mainly due to the fact that the probability that at least one of the peaks exceed the threshold increases as the expected number of users in a zone increases. This effect is significant and clearly observed at low SNRs. For the case of SNR $= -16\,\mathrm{dB}$ in Figure 5.6, the conventional detector achieves higher detection probabilities than SZ-GLRT-M after

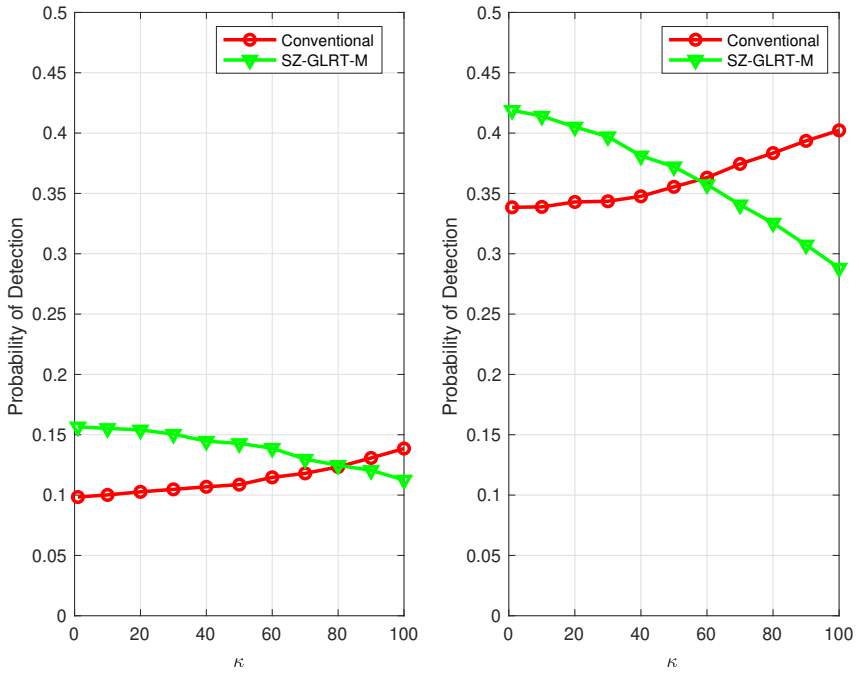

(a) $P_{fa} = 10^{-2}$ (b) $P_{fa} = 10^{-1}$

Figure 5.5: Detection probability versus κ at SNR $= -22\,\mathrm{dB}$ under TDL-C channel.

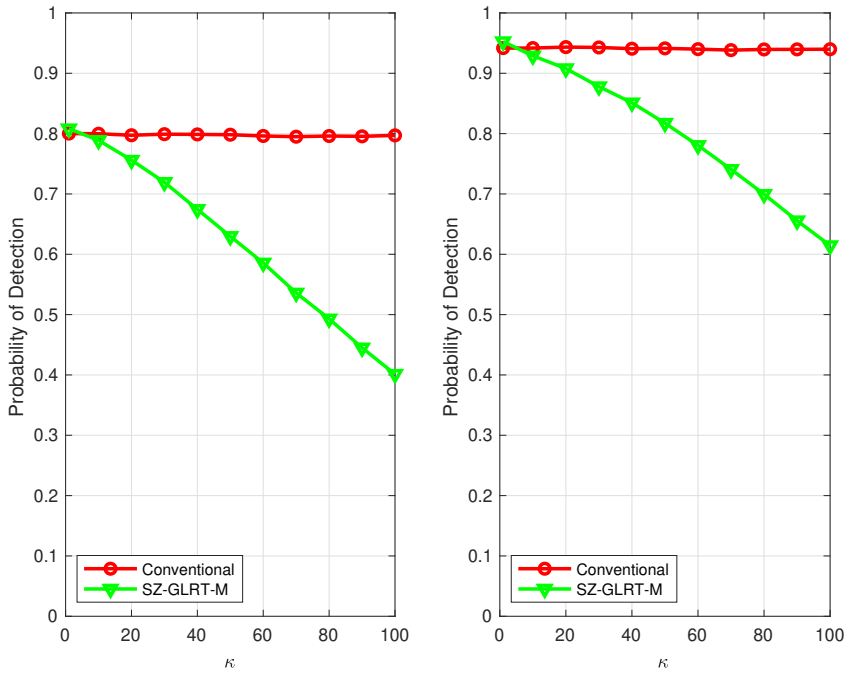

(a) $P_{fa} = 10^{-2}$ (b) $P_{fa} = 10^{-1}$

Figure 5.6: Detection probability versus κ at SNR $= -16$ dB under TDL-C channel.

$\kappa = 6$. Even this value is quite high for most practical applications as considered in many contribution reports [32] (commonly, $\kappa = 1$ is used). Furthermore, when Figures 5.5 and 5.6 are compared, it is noted that SZ-GLRT-M is outperformed by the conventional detector at lower κ values as SNR increases. This is also in accordance with Figure 5.2, where the SZ-GLRT performance approaches to that of the conventional detector as SNR increases.

Finally, the detection probability is plotted versus the SNR for two different arrival rates in Figure 5.7 and Figure 5.8 ($\kappa = 1$) for SZ-GLRT-M and the conventional detector, where $P_{fa} = 10^{-}2$. SZ-GLRT-M outperforms the conventional detector for the scenario in Figure 5.7, which corresponds to a low user arrival rate, i.e., $\kappa = 1$. On the other hand, for $\kappa = 5$, it is observed from Figure 5.8 that the conventional detector starts to outperform SZ-GLRT-M after an SNR of -14 dB.

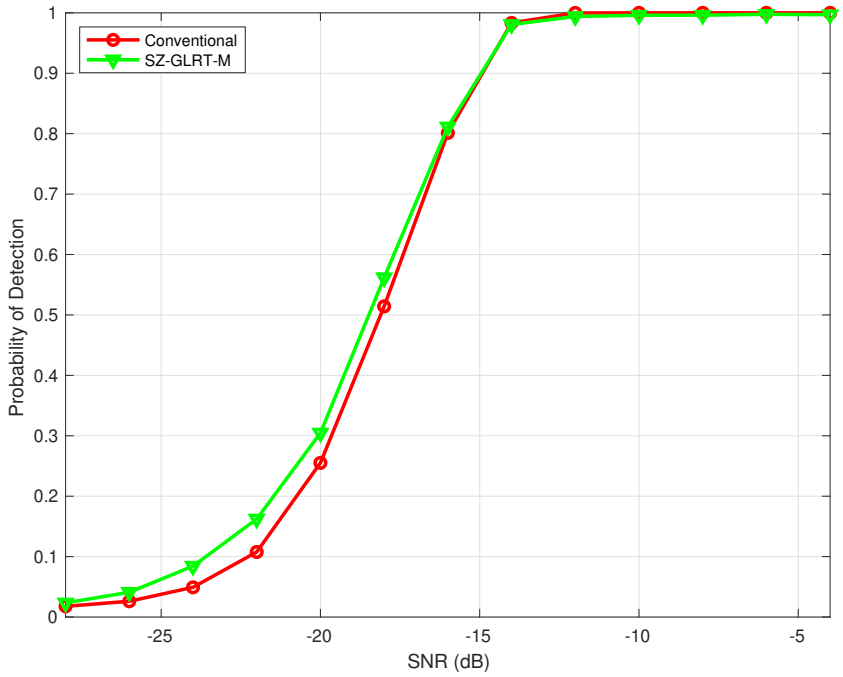

Figure 5.7: Detection probability versus SNR at $P_{fa} = 10^{-2}$ under TDL-C channel for $\kappa = 1$.

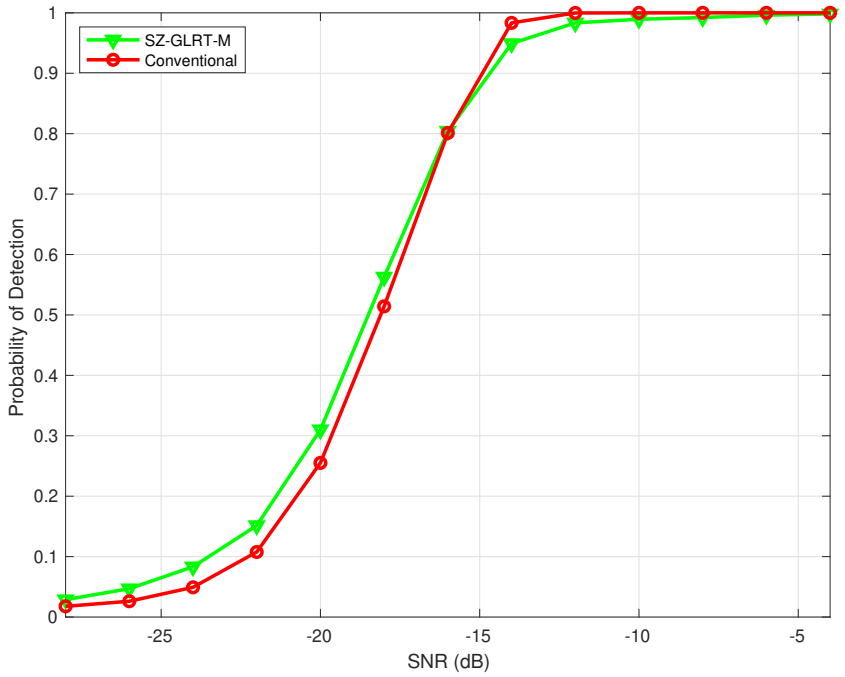

Figure 5.8: Detection probability versus SNR at $P_{fa} = 10^{-2}$ under TDL-C channel for $\kappa = 5$.

Chapter 6

Conclusion and Future Work

In this thesis, we have first briefly explained the evolution of mobile communication, discussed LTE and its characteristics, and mentioned the new features of 5G. Then, PRACH signal types, separation of them into zones, and detection of different cyclic shifted signals have been discussed. In addition, the importance of uplink synchronization detectors is explained as well as the challenges compared to downlink synchronization detectors. We have then also reviewed the conventional detector and emphasized its suboptimality. To provide improvements over the conventional detector, which performs point by point hypothesis testing, we have proposed a zone based GLRT approach for PRACH signal detection. For scenarios with at most one PRACH signal in each zone, we have first developed the Z-GLRT detector and then derived its low complexity version, called SZ-GLRT. For scenarios with multiple PRACH signals in a zone, we have proposed the SZ-GLRT-M detector. In addition, we have derived an ideal detector, the performance of which provides an upper bound for the performance of practical detectors. Via extensive simulations, it has been shown that Z-GLRT outperforms the conventional detector. On the other hand, the low-complexity detectors, SZ-GLRT and SZ-GLRT-M, achieve higher detection probabilities than the conventional detector for reasonably low false alarm probabilities and practical values of the UE arrival rate. Moreover, it has been shown that for high SNRs and very high values of UE arrival rates (which are not common), the conventional

detector can outperform SZ-GLRT-M. Overall, the SZ-GLRT-M detector can be used instead of the conventional detector in practical 5G applications unless very high UE arrival rates are expected.

As mentioned in Chapters 1 and Section 2, RACH process is performed in low SNRs because of the green network requirement and the battery limitations at the UE side. Additionally, there are many unknown parameters such as the index of the peak, noise variance, and channel coefficient. Due to these challenges, some papers and technical reports consider detection in the absence of interference inside the cell (the case that some UEs in the cell have different roots for Zadd-Off Chu sequences) in order to simplify the problem. This is a good approximation for the current RACH process system, since one can eliminate interference in the cell by choosing right values for the PRACH signal in the cell and in the neighboring cells [10]. However, this reduces the user capacity in the cell as explained in Chapter 2. Therefore, it is worth looking for a way to optimize the system by considering intra-cell interference. By the increase in the UE and IoT devices, this will be a crucial task for detecting devices in the cell. Currently there exist some proposed detectors for this case. Yet, they use exhaustive search for every possible interference scenario, and do not perform as well as expected for 5G [15]. Thus, this topic is an important candidate for future work.

As an alternative approach, machine learning tools (such as Q-learning) and neural networks can be employed for advanced problems related to the RACH process [33],[34]. The RACH process presents a complex problem with limited known data and observations. Please see [33], [34], [35] and [36] for some machine learning applications with promising performance results.

Currently, a new type of sequence is considered in the 5G literature. This sequence is called cover codes or quasi-orthogonal codes [16]. This new sequence type can increase user capacity if they are adopted as the new standard by 3GPP for the RACH process sequence. Basically, quasi-orthogonal codes use ZaddOff-Chu and m sequences by combining both of them to increase PRACH signal capacity [13]. Therefore, development of a new detector type for cover codes can be an interesting and practical topic for future work.

Bibliography

[1] S. Sesia, I. Toufik, and M. Baker, *LTE, The UMTS Long Term Evolution: From Theory to Practice*. Wiley Publishing, 2009.

[2] J. Chen, X. Ge, and Q. Ni, "Coverage and handoff analysis of 5G fractal small cell networks," *IEEE Transactions on Wireless Communications*, vol. 18, pp. 1263–1276, Feb. 2019.

[3] P. Han, Lei Guo, and Yejun Liu, "Green virtual network embedding framework based on zooming small cells in fiber-wireless access network for 5G," in *2017 19th International Conference on Transparent Optical Networks (ICTON)*, pp. 1–4, July 2017.

[4] T. M. B. Standard, "3GPP website." https://www.3gpp.org/, cited December 2019.

[5] A. Gohil, H. Modi, and S. K. Patel, "5G technology of mobile communication: A survey," in *2013 International Conference on Intelligent Systems and Signal Processing (ISSP)*, pp. 288–292, March 2013.

[6] M. Gundall, J. Schneider, H. D. Schotten, M. Aleksy, D. Schulz, N. Franchi, N. Schwarzenberg, C. Markwart, R. Halfmann, P. Rost, D. Wübben, A. Neumann, M. Düngen, T. Neugebauer, R. Blunk, M. Kus, and J. Grießbach, "5G as enabler for industrie 4.0 use cases: Challenges and concepts," in *2018 IEEE 23rd International Conference on Emerging Technologies and Factory Automation (ETFA)*, vol. 1, pp. 1401–1408, Sept. 2018.

[7] G. Baldini, S. Karanasios, D. Allen, and F. Vergari, "Survey of wireless communication technologies for public safety," *IEEE Communications Surveys and Tutorials*, vol. 16, pp. 619–641, Second Quarter 2014.

[8] X. Ge and W. Zhang, *5G Green Mobile Communication Networks*. Springer Singapore, 2019.

[9] M. Agiwal, A. Roy, and N. Saxena, "Next generation 5G wireless networks: A comprehensive survey," *IEEE Communications Surveys Tutorials*, vol. 18, pp. 1617–1655, Third Quarter 2016.

[10] S. Ahmadi, *5G NR: Architecture, Technology, Implementation, and Operation of 3GPP New Radio Standards*. Academic Press, 2019.

[11] S. P. E. Dahlman and J. Skold, *5G NR - The Next Generation Wireless Access Technology, San Diego, Elsevier Science & Technology*. Academic Press, 2018.

[12] B. Stiller, T. Bocek, F. Hecht, G. Machado, P. Racz, and M. Waldburger, "Physical channels and modulation," tech. rep., University of Zurich, Department of Informatics, Aug. 2010.

[13] R. Pitaval, B. M. Popovic, F. Berggren, and P. Wang, "Overcoming 5G PRACH Capacity Shortfall by Combining Zadoff-Chu and M-Sequences," in *2018 IEEE International Conference on Communications (ICC)*, pp. 1–6, May 2018.

[14] H. Saarnisaari, "Consecutive mean excision algorithms in narrowband or short time interference mitigation," in *Position Location and Navigation Symposium (PLANS 2004)*, pp. 447–454, April 2004.

[15] T. Kim, I. Bang, and D. K. Sung, "An enhanced PRACH preamble detector for cellular IoT communications," *IEEE Communications Letters*, vol. 21, pp. 2678–2681, Dec. 2017.

[16] B. M. Popovic, "Quasi-orthogonal supersets," in *2011 IEEE Information Theory Workshop*, pp. 155–159, Oct. 2011.

[17] A. Finger and H.-J. Zepernick, *Pseudo random Signal Processing: Theory and Application*. Wiley Publishing, 2005.

[18] S. Beyme and C. Leung, "Efficient computation of DFT of Zadoff-Chu sequences," *Electronics Letters*, vol. 45, pp. 461–463, April 2009.

[19] Y. Wen, W. Huang, and Z. Zhang, "CAZAC sequence and its application in LTE random access," in *2006 IEEE Information Theory Workshop (ITW 2006)*, pp. 544–547, Oct. 2006.

[20] M. Hua, M. Wang, K. W. Yang, and K. J. Zou, "Analysis of the frequency offset effect on Zadoff–Chu sequence timing performance," *IEEE Transactions on Communications*, vol. 62, pp. 4024–4039, Nov. 2014.

[21] G. Schreiber and M. Tavares, "5G new radio physical random access preamble design," in *2018 IEEE 5G World Forum (5GWF)*, pp. 215–220, July 2018.

[22] "TS 38.213 NR, Physical layer procedures for control," tech. rep., 3rd Generation Partnership Project, Sept. 2019.

[23] "TS 38.321 NR, Medium Access Control (MAC) protocol specification," tech. rep., 3rd Generation Partnership Project, Sept. 2019.

[24] "Physical channel design for 2-step RACH," tech. rep., Motorola Mobility, Jan. 2017.

[25] H. X. H. L. R. Wang, W. Chen and H. Lee, "Two step random access procedure," tech. rep., QUALCOMM Incorporated, 2018.

[26] S. Kim, K. Joo, and Y. Lim, "A delay-robust random access preamble detection algorithm for LTE system," in *2012 IEEE Radio and Wireless Symposium*, pp. 75–78, Jan. 2012.

[27] H. V. Poor, *An Introduction to Signal Detection and Estimation*. Springer, 2nd ed., 1994.

[28] S. M. Kay, *Fundamentals of Statistical Signal Processing: Detection Theory*. Prentice Hall, 2013.

[29] "3GPP TR 38.901. study on channel model for frequencies from 0.5 to 100 GHz," tech. rep., 3rd Generation Partnership Project, Sept. 2019.

[30] "3GPP TS 38.104. base station (BS) radio transmission and reception," tech. rep., 3rd Generation Partnership Project, Sept. 2019.

[31] "3GPP TS 38.101. user equipment (UE) radio transmission and reception," tech. rep., 3rd Generation Partnership Project, Sept. 2019.

[32] "R1-1701709, RACH preamble design for new radio," tech. rep., Huawei, 2017.

[33] S. K. Sharma and X. Wang, "Collaborative distributed Q-Learning for RACH congestion minimization in cellular IoT networks," *IEEE Communications Letters*, vol. 23, pp. 600–603, April 2019.

[34] L. M. Bello, P. Mitchell, D. Grace, and T. Mickus, "Q-learning Based Random Access with Collision free RACH Interactions for Cellular M2M," in *2015 9th International Conference on Next Generation Mobile Applications, Services and Technologies*, pp. 78–83, Sept. 2015.

[35] L. M. Bello, P. Mitchell, and D. Grace, "Application of Q-Learning for RACH Access to Support M2M Traffic over a Cellular Network," in *European Wireless 2014; 20th European Wireless Conference*, pp. 1–6, May 2014.

[36] L. M. Bello, P. Mitchell, and D. Grace, "Frame based back-off for Q-learning RACH access in LTE networks," in *2014 Australasian Telecommunication Networks and Applications Conference (ATNAC)*, pp. 176–181, Nov. 2014.

Appendix A

Derivation of (4.8)

Consider the likelihood function in (4.7), where m is the known index for the peak. Then, to find the MLEs for the unknown parameters, A and σ^2, we first obtain the log-likelihood function as

$$\log(p(r_1, r_2, \ldots, r_N)|\mathcal{H}_1) = -N\log(\pi) - N\log(\sigma^2) - \frac{|r_m - A|^2}{\sigma^2} - \frac{1}{\sigma^2}\sum_{i=1, i\neq m}^{N} |r_i|^2 \tag{A.1}$$

To maximize (A.1), its partial derivatives can be taken as follows:

$$\frac{\partial \log(p(r_1, r_2, ..., r_N|\mathcal{H}_1))}{\partial A} = 2|r_m - A| = 0 \tag{A.2}$$

$$\frac{\partial \log(p(r_1, r_2, ..., r_N|\mathcal{H}_1))}{\partial \sigma^2} = -\frac{N}{\sigma^2} + \frac{|r_m - A|^2}{\sigma^4} + \frac{1}{\sigma^4}\sum_{i=1, i\neq m}^{L} |r_i|^2 = 0 \tag{A.3}$$

Then, solving (A.2) and (A.3) yields the MLEs as $\tilde{A} = r_m$ and

$$\tilde{\sigma}_1^2 = \frac{\sum_{i=1, i\neq m}^{N} |r_i|^2}{N} \tag{A.4}$$

which is the estimator in (4.8).

Appendix B

Justification for (4.15)

Let the samples of the correlation signal in the subframe be denoted by $r_1, r_2, \ldots, r_L$. Suppose that there exist N_P PRACH signals and their indices are in set M_{N_P}. Assuming that set M_{N_P} is *known*, the probability density function of $r_1, r_2, \ldots, r_L$ under $\mathcal{H}_1$ (i.e., the likelihood function for $\mathcal{H}_1$) can be expressed as

$$p(r_1, r_2, \ldots, r_L|\mathcal{H}_1) = \frac{1}{(\pi\sigma^2)^L} e^{-\sum_{v\in M_{N_P}} \frac{|r_v - A_v|^2}{\sigma^2}} \prod_{i=1, i\notin M_{N_P}}^{L} e^{-\frac{|r_i|^2}{\sigma^2}}. \tag{B.1}$$

The log-likelihood function can be obtained from (B.1) as

$$\log(p(r_1, r_2, \ldots, r_L|\mathcal{H}_1)) = -L\log(\pi) - L\log(\sigma^2) - \frac{1}{\sigma^2}\sum_{v\in M_{N_P}} |r_v - A_v|^2 - \frac{1}{\sigma^2}\sum_{i=1, i\notin M_{N_P}}^{L} |r_i|^2. \tag{B.2}$$

Then, the likelihood equations are obtained as follows:

$$\frac{\partial \log(p(r_1, r_2, \ldots, r_L|\mathcal{H}_1))}{\partial A_v} = 2\sum_{v\in M_{N_P}} |r_v - A_v| = 0 \tag{B.3}$$

$$\frac{\partial \log(p(r_1, r_2, \ldots, r_L|\mathcal{H}_1))}{\partial \sigma^2} = -\frac{L}{\sigma^2} + \frac{1}{\sigma^4}\sum_{v\in M_{N_P}} |r_v - A_v|^2 + \frac{1}{\sigma^4}\sum_{i=1, i\notin M_{N_P}}^{L} |r_i|^2 = 0 \tag{B.4}$$

By solving (B.3) and (B.4), the MLE for σ^2 is derived as

$$\bar{\sigma}_1^2 = \frac{1}{L} \sum_{i=1, i \notin M_{N_P}}^{L} |r_i|^2 . \tag{B.5}$$

Since set M_{N_P}, which consists of the indices of the PRACH signals, is not known in practice, it can be estimated as the set of indices corresponding to the largest κ correlation values, i.e., set M_κ in Section 4.3, where κ is the average number of users in the subframe. Hence, by replacing M_{N_P} with M_κ, the estimator in (B.5) reduces to that in (4.15). Hence, (4.15) is a reasonable estimator to employ in practice, which would correspond to the MLE of σ^2 if M_κ were actually the set of indices for the PRACH signals.